Prompt K_short production in pp collisions at sqrt(s)=0.9 TeV

Physics Letters B 693 (2010) 69–80

Contents lists available at ScienceDirect

Physics Letters B

www.elsevier.com/locate/physletb

Prompt K^0_S production in pp collisions at $\sqrt{s} = 0.9$ TeV ☆,☆☆

LHCb Collaboration

ARTICLE INFO

Article history:
Received 18 August 2010
Accepted 24 August 2010
Available online 27 August 2010
Editor: W.-D. Schlatter

Dedicated to the memory of Werner Ruckstuhl, Peter Schlein and Tom Ypsilantis, who each played a fundamental role in the design of the experiment

Keywords:
Strangeness
Production
Cross-section
Luminosity
LHC
LHCb

ABSTRACT

The production of K^0_S mesons in pp collisions at a centre-of-mass energy of 0.9 TeV is studied with the LHCb detector at the Large Hadron Collider. The luminosity of the analysed sample is determined using a novel technique, involving measurements of the beam currents, sizes and positions, and is found to be $6.8 \pm 1.0\ \mu b^{-1}$. The differential prompt K^0_S production cross-section is measured as a function of the K^0_S transverse momentum and rapidity in the region $0 < p_T < 1.6$ GeV/c and $2.5 < y < 4.0$. The data are found to be in reasonable agreement with previous measurements and generator expectations.

1. Introduction

Strangeness production studies provide sensitive tests of soft hadronic interactions, as the mass of the strange quark is of the order of Λ_{QCD}. Strange-hadron production is suppressed, as a consequence, but still occurs in the non-perturbative regime. The hadronic production of K^0_S mesons has been studied by several experiments at a range of different centre-of-mass energies, both in pp and $p\bar{p}$ collisions (see for example [1–7]). The most recent measurements of K^0_S production at the Tevatron have shown deviations with respect to the expectations of hadronization models [6]. Strangeness production is also a topic of great interest in heavy ion physics, and measurements of this process in pp and $p\bar{p}$ collisions serve as reference point [7].

In this Letter measurements of prompt K^0_S production are presented using data collected with the LHCb detector in pp collisions at $\sqrt{s} = 0.9$ TeV, during the 2009 pilot run of the Large Hadron Collider (LHC). A K^0_S is defined to be prompt if it is directly produced in the pp collision, or if it appears in the decay chain of a non-weakly-decaying resonance (such as K^*) directly produced in the pp collision. The measurements are made in the rapidity interval $2.5 < y < 4.0$ and down to below 0.2 GeV/c transverse momentum with respect to the beam line. This is a region not explored at this energy by any previous experiment, and is complementary to the coverage of other LHC experiments. The determination of the prompt K^0_S production cross-section is normalized using an absolute measurement of the luminosity that relies on knowledge of the beam profiles.

The Letter is organized as follows. Section 2 gives a brief description of the LHCb detector and the configuration used to record data in December 2009 during the LHC pilot run. Section 3 gives an overview of the analysis strategy, the details of which are presented in the three following sections. Section 4 is dedicated to an explanation of the luminosity measurement, Section 5 presents the K^0_S candidate selection and Section 6 the determination of the K^0_S trigger and reconstruction efficiencies. The final results are discussed in Section 7 and compared with model expectations, before concluding in Section 8.

2. LHCb detector and 2009 data sample

The LHCb detector is a single-arm magnetic dipole spectrometer with a polar angular coverage with respect to the beam line of approximately 15 to 300 mrad in the horizontal bending plane, and 15 to 250 mrad in the vertical non-bending plane. The detector is described in detail elsewhere [8]. All subdetectors were fully operational and in a stable condition for the data that are analysed. For the measurements presented in this Letter the tracking detectors and trigger strategy are of particular importance.

A right-handed coordinate system is defined with its origin at the nominal pp interaction point, the z axis along the beam

☆ © CERN, for the benefit of the LHCb Collaboration.
☆☆ Date submitted: 2010-08-18 T17:08:28.

0370-2693/$ – see front matter 2010 Published by Elsevier B.V.
doi:10.1016/j.physletb.2010.08.055

line and pointing towards the magnet, and the y axis pointing upwards. Beam-1 (beam-2) travels in the direction of positive (negative) z.

The LHCb tracking system consists of the Vertex Locator (VELO) surrounding the pp interaction region, a tracking station (TT) upstream of the dipole magnet, and three tracking stations (T1–T3) downstream of the magnet. Particles traversing from the interaction region to the downstream tracking stations experience a bending-field integral of 3.7 Tm on average.

The VELO consists of silicon microstrip modules, providing a measure of the radial and azimuthal coordinates, r and ϕ, distributed in 23 stations arranged along the beam direction. The first two stations at the most upstream z positions are instrumented to provide information on the number of visible interactions in the detector at the first level of the trigger ('pile-up detector'). The VELO is constructed in two halves (left and right), movable in the x and y directions so that it can be centred on the beam. During stable beam conditions the two halves are located at their nominal closed position, with active silicon at 8 mm from the beams, providing full azimuthal coverage. During injection and beam adjustments the two halves are moved apart horizontally to a retracted position away from the beams.

The TT station also uses silicon microstrip technology. The downstream tracking stations T1–T3 have silicon microstrips in the region close to the beam pipe (Inner Tracker, IT), whereas straw tubes are employed in the outer region (Outer Tracker, OT).

During the 2009 run, low intensity beams collided in LHCb at the LHC injection energy, corresponding to a total energy of 0.9 TeV. Due to the dipole magnetic field the beams have a crossing angle that results in the pp centre-of-mass frame moving with velocity $0.0021c$ in the $-x$ direction. Both the beam sizes and crossing angle were larger than those designed for high-energy collisions. In order not to risk the safety of the VELO, the 2009 data were recorded with the two VELO halves positioned 15 mm away from their nominal data-taking position (VELO partially open), resulting in a reduced azimuthal coverage. For this run, the magnetic dipole field was pointing downwards.

The bulk of the data presented here were collected in a series of LHC fills with the following two sets of beam conditions. The first configuration contained four bunches per beam, spaced by more than 8 μs, with two colliding and two non-colliding bunches, and a total peak beam intensity of about 1.8×10^{10} protons per bunch. The second configuration contained 16 bunches per beam, spaced by more than 2 μs, with eight colliding and eight non-colliding bunches, and a total peak beam intensity of about 1.3×10^{10} protons per bunch. The nominal LHC injection optical function at the interaction point was used ($\beta^* = 10$ m).

A trigger strategy was deployed to provide high efficiency for pp inelastic interactions and for beam collisions with the residual gas in the vacuum chamber. The latter class of events is a necessary ingredient for the luminosity analysis. Events were collected for three bunch-crossing types: two colliding bunches (bb), beam-1 bunch with no beam-2 bunch ($b1$), and beam-2 bunch with no beam-1 bunch ($b2$). The first two categories of crossings, which produce particles in the forward ($+z$) direction, were triggered using calorimeter information: a 2×2 cluster with more than 240 MeV of transverse energy in the Hadron Calorimeter (HCAL) and at least three hits in the 6016 cells of the Scintillator Pad Detector (SPD) at the entrance to the calorimeter were required. Events containing a track in the muon system with transverse momentum above 480 MeV/c were also triggered. Crossings of the type $b2$, which produce particles in the backward direction only, were triggered by demanding a hit multiplicity of more than seven in the pile-up detector.

The visible collision rate for a single bunch pair was about 10 Hz and the acquired $b1$ ($b2$) rate for a single bunch was approximately 0.015 Hz (0.002 Hz), in agreement with the measured residual pressure and VELO acceptance. A sample of 424 193 events triggered in bb crossings is used in the K^0_S analysis.

3. Analysis strategy

All K^0_S candidates are reconstructed in the $\pi^+\pi^-$ decay mode, using only events triggered by the calorimeter. Contributions from secondary interactions in the detector material or from the decay of long-lived particles are suppressed by requiring the K^0_S candidates to point back to the pp-collision point. No attempt is made to separate the contributions from K^0_S mesons produced in diffractive and non-diffractive processes.

Due to the long K^0_S lifetime and partially open VELO position, only a small fraction of the K^0_S daughter tracks traversing the spectrometer leave a signal in the VELO. Therefore, two paths are followed for the K^0_S reconstruction and selection:

a) Downstream-track selection:
Tracks reconstructed only with hits in the TT and T1–T3 stations (called downstream tracks) are combined, without using the VELO. The origin of the K^0_S is taken as the point on the z axis that is closest to the reconstructed flight vector of the K^0_S candidate. This point is taken as an estimate of the primary vertex (PV), and is referred to as the 'pseudo-PV'.

b) Long-track selection:
K^0_S candidates are formed with tracks leaving hits in the VELO and in the T stations (called long tracks). If available, measurements in the TT are added to the tracks. The PV is reconstructed from tracks seen in the detector, using VELO information whenever available.

The analysis is performed in bins of K^0_S phase space. The kinematic variables used are the K^0_S transverse momentum $p_T = \sqrt{p_x^2 + p_y^2}$ and the rapidity $y = \frac{1}{2}\ln((E + p_z)/(E - p_z))$, where $(E, \vec{p})$ is the K^0_S four-momentum in the pp centre-of-mass system. For a given bin i in p_T and y, the prompt K^0_S production cross-section is calculated as

$$\sigma_i = \frac{N_i^{\text{obs}}}{\epsilon_i^{\text{trig/sel}} \epsilon_i^{\text{sel}} L_{\text{int}}}, \tag{1}$$

where N_i^{obs} is the number of observed $K^0_S \to \pi^+\pi^-$ signal decays with reconstructed p_T and y in bin i, ϵ_i^{sel} the reconstruction and selection efficiency, $\epsilon_i^{\text{trig/sel}}$ the trigger efficiency on selected events, and L_{int} the integrated luminosity. The number of signal events N_i^{obs} is obtained from the mass distributions of the K^0_S candidates.

The reconstruction and selection efficiency is estimated from a fully-simulated Monte Carlo (MC) sample of single pp collisions as

$$\epsilon_i^{\text{sel}} = \frac{N_i^{\text{sel}}}{N_i^{\text{prompt}}}, \tag{2}$$

where N_i^{sel} is the number of $K^0_S \to \pi^+\pi^-$ signal decays selected in the untriggered MC sample with reconstructed p_T and y in bin i (extracted using the same procedure as in the data), and where N_i^{prompt} is the number of generated prompt K^0_S mesons with generated p_T and y in bin i. This efficiency includes the geometrical acceptance, as well as the reconstruction and selection efficiencies. It also incorporates all corrections related to the following effects: secondary interactions of K^0_S in the material, $K^0_S \to \pi^+\pi^-$ branching fraction, decay in flight and secondary interaction of the decay

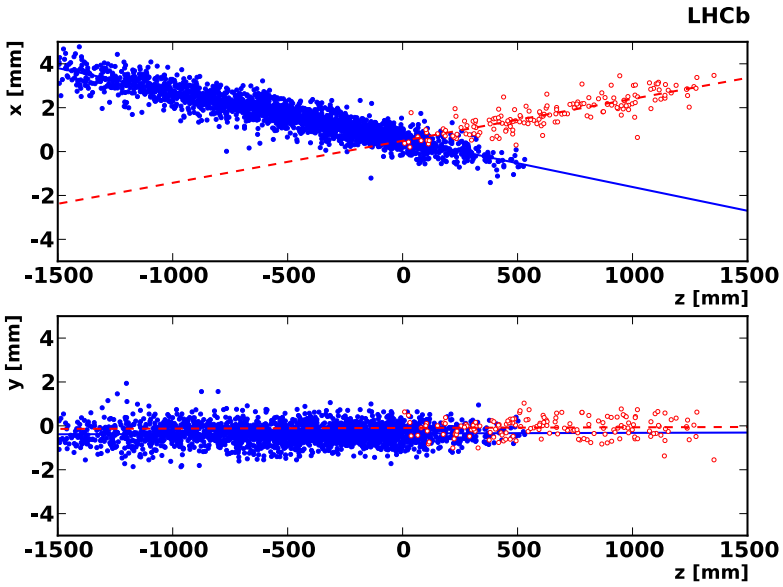

Fig. 1. Distributions in the horizontal (top) and vertical (bottom) planes of the reconstructed vertices in $b1$ (blue filled circles and solid fit line) and $b2$ (red open circles and dashed fit line) crossings in one fill. (For interpretation of the references to colour in this figure legend, the reader is referred to the web version of this Letter.)

products, non-prompt K^0_S production and finite resolution of the p_T and y observables.

The trigger efficiency is estimated using the same MC events. However, since the efficiency depends on the global event properties, the MC events are weighted to reproduce the observed track multiplicity in the selected signal events. Then

$$\epsilon_i^{\text{trig/sel}} = \frac{Y_i^{\text{trig/sel}}}{Y_i^{\text{sel}}} \tag{3}$$

is computed, where $Y_i^{\text{trig/sel}}$ and Y_i^{sel} are the weighted MC signal yields extracted after and before the trigger cuts are applied.

The integrated luminosity L_{int} is determined using a novel 'beam imaging' method [9], taking advantage of proton collisions with the residual gas in the interaction region and of the excellent vertexing capability of the VELO. The beam profiles and positions are reconstructed using tracks produced in beam–gas and beam–beam collisions. Combining this information with bunch current measurements from the LHC machine yields a direct measurement of the integrated luminosity.

4. Luminosity determination

In the relativistic approximation, the average instantaneous luminosity produced by one pair of colliding bunches can be expressed as [10]

$$L = 2cn_1n_2 f \cos^2\theta \int \rho_1(x,y,z,t)\rho_2(x,y,z,t)\,\mathrm{d}x\,\mathrm{d}y\,\mathrm{d}z\,\mathrm{d}t, \tag{4}$$

where n_i are the number of protons in bunch i ($i = 1, 2$), $f = 11.245$ kHz is the LHC revolution frequency, θ is the half crossing angle of the beams, and $\rho_i(x,y,z,t)$ is the density of bunch i normalized as $\int \rho_i(x,y,z,t)\,\mathrm{d}x\,\mathrm{d}y\,\mathrm{d}z = 1$ at all times t. The overlap integral in Eq. (4) is taken over the duration of one bunch crossing. Tracks measured in the VELO allow vertices from beam–gas and beam–beam collisions to be reconstructed for each pair of bunches. From the distributions of these vertices, and assuming the gas density to be uniform in any plane transverse to the beams, the positions, angles and sizes of the bunches are measured, and their overlap integral is computed. The numbers of protons per bunch are determined with the LHC machine instrumentation, enabling an absolute normalization of the luminosity. The total luminosity is then obtained as the sum of the estimates for each pair of colliding bunches in the machine.

The beam crossing angle is limited to the horizontal plane. No correlation between the transverse coordinates is observed at the level of precision needed for this analysis, thus the x and y projections can be factorized. The bunch shapes are well described by Gaussian distributions in all three dimensions, characterized in the x–y plane at the time of crossing by their width σ_{ij} and their mean position μ_{ij} ($j = x, y$), and by their average longitudinal width σ_z, assumed to be equal for both beams. With these approximations and for small crossing angle, Eq. (4) can be rewritten as

$$L = \frac{n_1n_2 f}{2\pi\sqrt{1+2(\theta\sigma_z)^2/(\sigma_{1x}^2+\sigma_{2x}^2)}} \prod_{j=x,y} \frac{1}{\sqrt{\sigma_{1j}^2+\sigma_{2j}^2}} \times \exp\left(-\frac{1}{2}\frac{(\mu_{1j}-\mu_{2j})^2}{\sigma_{1j}^2+\sigma_{2j}^2}\right). \tag{5}$$

The observables σ_{ij} and μ_{ij} are extracted from the transverse distributions of the beam–gas vertices reconstructed in the bb crossings of the colliding bunch pair with a z coordinate satisfying $-1000 < z < -200$ mm ($200 < z < 1000$ mm) for $i = 1$ ($i = 2$). These transverse distributions are obtained by projecting the reconstructed vertex positions onto a plane perpendicular to the corresponding beam direction. As illustrated in Fig. 1, the beam directions, and hence also the half crossing angle θ, are obtained from straight-line fits through the measured positions of vertices reconstructed in $b1$ and $b2$ crossings of other non-colliding bunches. The observed half crossing angle of $\theta = 2.1 \pm 0.1$ mrad in the horizontal plane is in agreement with the expected value.

In addition, the distribution of pp-collision vertices, produced by the colliding bunch pair and identified by requiring $-150 < z < 150$ mm, can be used to measure the parameters of the luminous region. Its position μ_j and transverse width σ_j,

$$\mu_j = \frac{\mu_{1j}\sigma_{2j}^2 + \mu_{2j}\sigma_{1j}^2}{\sigma_{1j}^2+\sigma_{2j}^2} \quad \text{and} \quad \sigma_j^2 = \frac{\sigma_{1j}^2\sigma_{2j}^2}{\sigma_{1j}^2+\sigma_{2j}^2} \quad (j = x, y) \tag{6}$$

Table 1
Parameters describing the vertex resolution functions defined in Eqs. (7) and (8). The quoted errors include statistical and systematic uncertainties. The parameters f_j and r_j were fixed in the fits, and hence have no uncertainties.

	f_j	r_j	s_j^{track} [μm]	δ_j	b_{1j}	m_{1j} [m^{-1}]	b_{2j}	m_{2j} [m^{-1}]
x	0.9	0.32	177 ± 7	5.9 ± 1.1	1.18 ± 0.07	-0.86 ± 0.30	0.83 ± 0.14	$+0.77 \pm 0.24$
y	0.9	0.36	164 ± 6	3.7 ± 1.1	1.24 ± 0.08	-0.57 ± 0.16	0.85 ± 0.14	$+0.77 \pm 0.24$

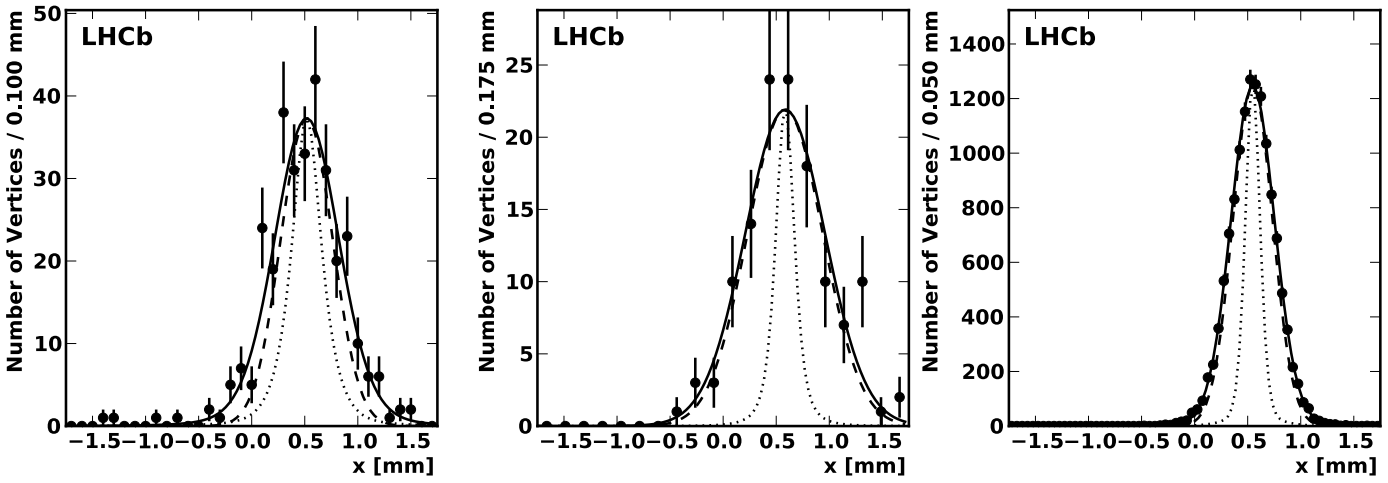

Fig. 2. Measured profiles of beam-1, beam-2 and luminous region (from left to right) in the horizontal direction x, in bb crossings of one pair of colliding bunches in one fill. The solid curve is a fit to the observed distributions, the dotted curve represents the vertex resolution, and the dashed curve shows the underlying distributions after deconvolution of the vertex resolution.

can be used to constrain the bunch observables. Owing to the higher statistics of pp collisions compared to beam–gas interactions, the constraints of Eq. (6) provide the most significant input to the overlap integral.

The longitudinal bunch size σ_z is extracted from the longitudinal distribution of the pp-collision vertices. Because σ_z is approximately 200 times larger than σ_{ix}, the crossing angle reduces the luminosity by a non-negligible factor equal to the first square root term in Eq. (5). For the fill used to determine the absolute luminosity, this factor is estimated to be 1.087 ± 0.012.

The vertex resolutions need to be measured since they are of the same order as the bunch sizes. This is achieved by comparing, on an event-by-event basis, the reconstructed vertex positions obtained from two independent sets of tracks. In each event, the sample of available tracks is randomly split into two sets of equal multiplicity, and the event is kept only if exactly one vertex is reconstructed for each set. In this case the two vertices are assumed to originate from the same interaction. The vertex resolution for each coordinate is obtained as the width of the distribution of the difference in position between the two reconstructed vertices divided by $\sqrt{2}$. A systematic study of the vertex resolutions in both x and y is then performed as a function of the number of tracks N contributing to the vertex, of the crossing type, and of the z coordinate of the vertex. The resolution functions are found to be well parametrized by a double Gaussian function

$$R_j(N,z) = f_j G\big(s_j(N,z)\big) + (1-f_j) G\big(s_j(N,z)/r_j\big) \quad (j = x, y), \tag{7}$$

where f_j is the fraction of events in the first Gaussian function, r_j is the ratio of the widths of the two Gaussian functions, and $G(s_j(N,z))$ is a Gaussian function centred at zero with width

$$s_j^{bb}(N,z) = N^{-0.5+\delta_j/N^2} s_j^{\text{track}} \quad \text{for beam–beam,}$$

$$s_j^{i}(N,z) = (b_{ij} + m_{ij} z) s_j^{bb}(N,z) \quad \text{for beam–gas} \quad (i = 1, 2) \quad (j = x, y). \tag{8}$$

The parameters s_j^{track} describe the per-track resolutions, δ_j specify the dependence on the number of tracks, while b_{ij} and m_{ij} model the linear z dependence for beam–gas vertices. The validity of this parametrization has been verified with MC simulation studies. The systematic uncertainties on the parameters are estimated from the level of agreement in that check. The final set of resolution parameters is given in Table 1. The resolution is found to be better in y than in x, which is expected from the partial VELO opening described in Section 2.

For both transverse coordinates, each sample of vertices (defined for every colliding bunch pair in each fill) is fitted with convolutions of the Gaussian beam shapes with the resolution function of Eq. (7). This fit is performed with all three types of interactions. With the constraints of Eq. (6), this yields directly the position μ_{ij} and Gaussian width σ_{ij} of the underlying distributions. Some example distributions are shown in Fig. 2. The systematic errors on the results are estimated by varying the resolution parameters within their total uncertainties.

The remaining ingredients needed for the direct luminosity measurement are the bunch intensities. The LHC is equipped with two systems of beam current transformers (BCT) [11]. A DC–BCT system provides an ungated measurement of the total beam current, while a fast-BCT system is gated to measure the current induced on a bunch-by-bunch basis. The individual bunch intensities are obtained from these fast-BCT readings, but constraining their sum to the DC–BCT measurements. At the low intensities of the 2009 pilot run, the offset in the DC–BCT digitization is non-negligible and is corrected by averaging the readings in the periods without circulating beam just before and after a fill.

The method described above was used to measure the luminosity in four different machine fills. Two of those fills were relatively

short and the third was taken before optimization of the beam alignment. The remaining fill, taken under optimal conditions and representing approximately 25% of the sample used for the K^0_S production study, is chosen to determine the absolute normalization of the luminosity for the data set used for the K^0_S analysis. The other three fills yield less precise but consistent results. The integrated luminosity for the data set used for the K^0_S selection, $L_{\rm int} = 6.8 \pm 1.0\ \mu{\rm b}^{-1}$, is obtained by scaling with the number of pp interaction vertices measured with the VELO. The relative uncertainty on this result comprises contributions from the measurements of the beam intensities (12%), widths (5%), relative positions (3%) and crossing angle (1%). This is the most precise determination of the luminosity for the 2009 LHC pilot run. The limiting uncertainty on the beam intensity is expected to improve in the future.

5. K^0_S selection and signal extraction

In the downstream-track selection, a K^0_S candidate is formed from any combination of two oppositely-charged downstream tracks, assumed to be pions, satisfying the requirements listed in the top part of Table 2. The pseudo-PV was defined in Section 3, and $\theta_{\rm pointing}$ is the angle between the K^0_S momentum vector and the direction joining the pseudo-PV and the K^0_S decay vertex.

In the long-track selection, primary vertices are reconstructed from at least three tracks. Each K^0_S candidate formed from long tracks is associated with the PV that minimizes its impact parameter and the requirements listed in the bottom part of Table 2 are applied. The variable ν is similar to a Fisher discriminant formed with the logarithms of the impact parameters; it is defined as $\nu = \ln[(I_+ I_-)/(I_0 I_1)]$. Here I_+, I_- and I_0 are the impact parameters of each of the two tracks and of the K^0_S candidate with respect to their closest PV, respectively, and the value of I_1 is fixed to 1 mm.

Table 2
$K^0_S \to \pi^+\pi^-$ selection requirements.

Variable	Requirement
Downstream-track selection	
Each π-track momentum	> 2 GeV/c
Each π-track transverse momentum	> 0.05 GeV/c
Each track fit χ^2/ndf	< 25
Distance of closest approach of each π-track to the z axis	> 3 mm
K^0_S decay vertex fit χ^2/ndf	< 25
z of K^0_S decay vertex	< 2200 mm
$\lvert z\rvert$ of pseudo-PV	< 150 mm
$\cos\theta_{\rm pointing}$	> 0.99995
K^0_S proper time ($c\tau$)	> 5 mm
Long-track selection	
$\lvert z\rvert$ of associated PV	< 200 mm
Each track fit χ^2/ndf	< 25
K^0_S decay vertex χ^2/ndf	< 100
$z(K^0_S) - z({\rm PV})$	> 0 mm
Variable ν related to impact parameters	> 2

Mass distributions are obtained for both bb crossings and $b1$ crossings. In order to keep only the contribution arising from pp collisions, the $b1$ mass distribution is subtracted, after proper normalization, from the bb mass distribution. The normalization factor is 0.908 ± 0.015, averaged over the entire sample used for this analysis. It is obtained from the ratio of the number of interaction vertices reconstructed in bb and $b1$ crossings in the region $z < -200$ mm where no pp collision can take place. This beam–gas subtraction removes about 1.2% of the K^0_S signal.

The beam–gas subtracted mass distributions are shown in Fig. 3 for all selected K^0_S candidates. A χ^2 fit is made, describing the background with a linear function and the signal with the sum of two Gaussian functions of common mean value, with all parameters left free. It gives a total K^0_S signal yield of 4801 ± 84 (1140 ± 35), a mean mass value of 497.12 ± 0.14 MeV/c^2 (497.43 ± 0.14 MeV/c^2), and an average resolution of 9.2 MeV/c^2 (5.5 MeV/c^2) for the downstream-track (long-track) selection. Quoted uncertainties are statistical only. The mass values are close to the known K^0_S mass value of 497.61 ± 0.02 MeV/c^2 [12], reflecting the current status of the mass-scale calibration. In the long-track selection, the statistics are lower than in the downstream-track selection, but the background level is lower and the mass resolution is significantly better.

The beam–gas subtraction and signal yield extraction are repeated for each bin in $p_{\rm T}$ and y, leading to the results shown in Table 3. The systematic uncertainties on the extraction of these yields are obtained by comparing the yields from single and double Gaussian signal fits and from side-band subtraction to the expected yield in a Monte Carlo sample of comparable statistics to the data set. Additionally the fitted and side-band subtracted yields are compared, and an alternate (exponential) background model is used in the mass fits. The largest observed deviation in any of these studies is taken as systematic uncertainty. For the long-track selection, where the yields are lower, the central value is obtained from the side-band subtraction method assuming a linear background.

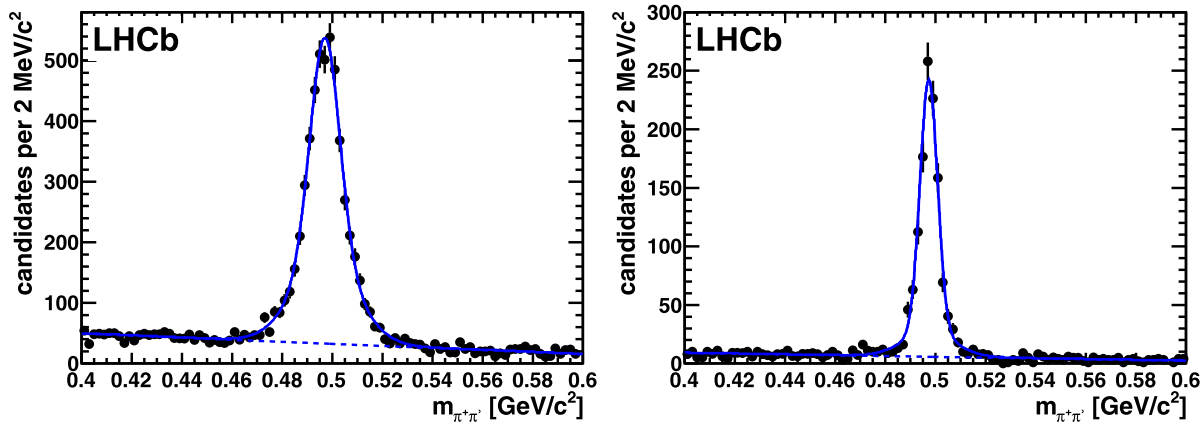

Fig. 3. Mass distributions of all selected K^0_S candidates, in the downstream-track (left) and long-track (right) selections. The points are the beam–gas subtracted data and the curves are the result of the fits described in the text.

6. Efficiency estimation

A sample of fully simulated events is used to estimate the reconstruction and selection efficiency $\epsilon_i^{\rm sel}$ in each $p_{\rm T}$ and y bin. Single pp collisions are generated with the PYTHIA 6.4 program [13] and the generated particles are tracked through the detector with the GEANT 4 package [14], taking into account the details of the geometry and material composition of the detector. The simulation of the detector response is tuned to reproduce test beam results [8]. In terms of dead and noisy channels, the simulation reflects the detector status of the data set used in this analysis.

Residual misalignments of the tracking stations and edge-effects of cell efficiencies in the Outer Tracker are not perfectly described in the MC sample, resulting in an overestimation of the tracking efficiency. To incorporate these effects, we compare for each detector unit the hit content of the tracks in the data and MC samples and randomly remove hits in the simulation until we achieve agreement in all subdetector components and phase-space regions. The MC sample modified in this way is the nominal MC sample, used throughout the analysis.

Table 3
Number of observed beam–gas subtracted $K_S^0 \to \pi^+\pi^-$ signal decays, as extracted in the downstream- and long-track selections for each bin of transverse momentum $p_{\rm T}$ and rapidity y. The first quoted uncertainty is statistical and the second systematic. The latter is uncorrelated across bins. A dash indicates that the statistics were insufficient to determine a result in that bin.

$p_{\rm T}$ [GeV/c]	$2.5 < y < 3.0$	$3.0 < y < 3.5$	$3.5 < y < 4.0$
Downstream-track selection			
0.0–0.2	–	$73 \pm 10 \pm 2$	$40 \pm 8 \pm 1$
0.2–0.4	–	$278 \pm 21 \pm 6$	$288 \pm 21 \pm 10$
0.4–0.6	$147 \pm 15 \pm 4$	$428 \pm 24 \pm 7$	$388 \pm 21 \pm 10$
0.6–0.8	$202 \pm 16 \pm 1$	$379 \pm 22 \pm 8$	$332 \pm 21 \pm 8$
0.8–1.0	$176 \pm 15 \pm 1$	$213 \pm 16 \pm 6$	$217 \pm 17 \pm 1$
1.0–1.2	$113 \pm 11 \pm 1$	$173 \pm 14 \pm 1$	$111 \pm 12 \pm 4$
1.2–1.4	$94 \pm 11 \pm 2$	$90 \pm 10 \pm 0$	$32 \pm 8 \pm 0$
1.4–1.6	$56 \pm 8 \pm 2$	$64 \pm 8 \pm 3$	$20 \pm 5 \pm 1$
Long-track selection			
0.0–0.2	$17 \pm 5 \pm 2$	$34 \pm 7 \pm 3$	–
0.2–0.4	$31 \pm 6 \pm 2$	$75 \pm 9 \pm 4$	–
0.4–0.6	$63 \pm 8 \pm 6$	$121 \pm 12 \pm 3$	$41 \pm 7 \pm 1$
0.6–0.8	$64 \pm 8 \pm 2$	$134 \pm 12 \pm 3$	$65 \pm 9 \pm 5$
0.8–1.0	$50 \pm 7 \pm 2$	$91 \pm 10 \pm 2$	$53 \pm 8 \pm 4$
1.0–1.2	$30 \pm 6 \pm 1$	$40 \pm 7 \pm 5$	$35 \pm 7 \pm 2$
1.2–1.4	$16 \pm 4 \pm 0$	$33 \pm 6 \pm 5$	$27 \pm 5 \pm 6$
1.4–1.6	$8 \pm 3 \pm 0$	$19 \pm 5 \pm 3$	$14 \pm 4 \pm 2$

To assign systematic uncertainties on the efficiencies obtained in this MC sample the single track-finding efficiencies were measured. The VELO efficiency is obtained by using reconstructed tracks in the TT and in the T1–T3 stations and checking for an associated track segment in the VELO. Similarly the TT and T1–T3 station efficiencies are tested by reconstructing tracks using VELO and HCAL information. For downstream tracks with a $p_{\rm T}$ larger than 0.2 GeV/c agreement between the track-finding efficiencies in data and in the Monte Carlo sample is observed within the statistical uncertainties of approximately 3%. Below 0.2 GeV/c, the ratio of efficiencies in data and MC is found to be 0.85 ± 0.12. As a conservative approach 3% (15%) uncertainties for the reconstruction efficiency of tracks with a $p_{\rm T}$ larger (smaller) than 0.2 GeV/c are assigned. Propagating these uncertainties to the K_S^0 reconstruction efficiency results in correlated systematic uncertainties of up to 17% for the lowest K_S^0 $p_{\rm T}$ bins of the downstream-track selection.

The systematic uncertainty on the K_S^0 selection efficiency is obtained by comparing, in data and MC, the selection efficiency relative to a preselection. This preselection is close to 90% efficient for downstream-track selected signal events in MC.

If the reconstruction and selection efficiency varies strongly within a given bin of phase space, the average value estimated with MC will depend on the assumed production spectrum within the bin. The extraction of the efficiency-corrected yield in each bin is therefore repeated using efficiencies in four sub-bins rather than an average efficiency, and the difference with respect to the nominal result is taken as an uncorrelated systematic uncertainty. The size of this effect varies between 0 and 20%. The largest uncertainties are obtained in bins at the limit of the acceptance.

The fraction of non-prompt K_S^0 signal in the selected MC sample is found to be 0.6%. By definition, this is corrected for in the efficiencies defined in Eq. (2). Because the correction is so small, even doubling this contribution would have no significant impact on the final result. Similarly, the systematic uncertainty due to material interactions, assuming a conservative $\pm 10\%$ variation of the known detector material, is found to be negligible.

The trigger efficiency $\epsilon_i^{\rm trig/sel}$ for selected signal events depends on the track multiplicity. As outlined in Section 3, $\epsilon_i^{\rm trig/sel}$ is obtained after weighting the previously-defined nominal MC sample in order to reproduce, in selected signal events, the track multiplicity observed in the data (see Fig. 4 (left)). This re-weighting is only applied for the determination of the trigger efficiency, as the reconstruction and selection efficiency has been shown not to de-

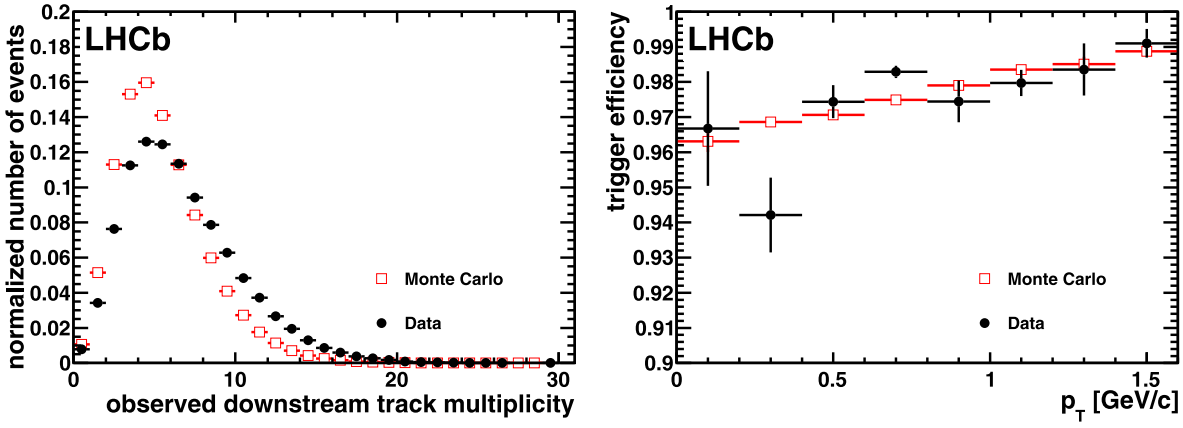

Fig. 4. Left: Downstream track multiplicity for events containing a signal K_S^0, in data (black filled circles) and MC (red open squares), normalized to unit area. Right: Trigger efficiency for events containing a signal K_S^0 decay in the downstream-track selection, as a function of the K_S^0 $p_{\rm T}$, estimated both in data (black filled circles) and MC (red open squares), using Eq. (9). (For interpretation of the references to colour in this figure legend, the reader is referred to the web version of this Letter.)

Table 4
Total efficiencies (in %) in bins of transverse momentum p_T and rapidity y for the two selections. The first uncertainty is uncorrelated, including the statistical uncertainty from MC, and the second is at least partially correlated across bins.

p_T [GeV/c]	$2.5 < y < 3.0$	$3.0 < y < 3.5$	$3.5 < y < 4.0$
Downstream-track selection			
0.0–0.2	–	$3.4 \pm 0.5 \pm 0.5$	$3.0 \pm 0.6 \pm 0.3$
0.2–0.4	–	$7.3 \pm 0.2 \pm 0.8$	$7.4 \pm 0.2 \pm 1.0$
0.4–0.6	$3.5 \pm 0.4 \pm 0.4$	$11.8 \pm 0.2 \pm 0.9$	$12.0 \pm 0.2 \pm 0.9$
0.6–0.8	$7.4 \pm 0.3 \pm 0.5$	$15.0 \pm 0.2 \pm 1.2$	$15.1 \pm 0.2 \pm 1.2$
0.8–1.0	$11.1 \pm 0.2 \pm 0.9$	$17.1 \pm 0.2 \pm 1.3$	$15.8 \pm 0.4 \pm 1.2$
1.0–1.2	$14.5 \pm 0.5 \pm 1.2$	$18.7 \pm 0.5 \pm 1.4$	$15.1 \pm 0.4 \pm 1.2$
1.2–1.4	$16.2 \pm 0.4 \pm 1.2$	$18.9 \pm 0.5 \pm 1.5$	$13.6 \pm 1.1 \pm 1.0$
1.4–1.6	$17.8 \pm 0.6 \pm 1.3$	$19.1 \pm 0.7 \pm 1.5$	$12.6 \pm 1.2 \pm 0.9$
Long-track selection			
0.0–0.2	$0.8 \pm 0.0 \pm 0.2$	$2.0 \pm 0.1 \pm 0.4$	–
0.2–0.4	$0.7 \pm 0.1 \pm 0.1$	$2.0 \pm 0.1 \pm 0.4$	–
0.4–0.6	$1.2 \pm 0.0 \pm 0.2$	$3.7 \pm 0.1 \pm 0.6$	$1.3 \pm 0.3 \pm 0.2$
0.6–0.8	$1.9 \pm 0.1 \pm 0.3$	$4.9 \pm 0.1 \pm 0.6$	$2.9 \pm 0.1 \pm 0.4$
0.8–1.0	$2.6 \pm 0.1 \pm 0.3$	$5.6 \pm 0.1 \pm 0.7$	$4.1 \pm 0.5 \pm 0.5$
1.0–1.2	$2.8 \pm 0.1 \pm 0.3$	$6.1 \pm 0.5 \pm 0.6$	$4.3 \pm 0.3 \pm 0.4$
1.2–1.4	$2.7 \pm 0.2 \pm 0.2$	$5.7 \pm 0.5 \pm 0.5$	$5.1 \pm 0.6 \pm 0.6$
1.4–1.6	$2.8 \pm 0.3 \pm 0.2$	$5.7 \pm 0.5 \pm 0.5$	$5.4 \pm 0.5 \pm 0.5$

pend on the track multiplicity. The trigger efficiency is found to be greater than 95% in every phase-space bin. As a cross check, it is also extracted directly from data, using a method that exploits the fact that signal events can be triggered by the K^0_S daughters (trigger on signal, TOS) or by the rest of the event (trigger independent of signal, TIS), with a very large overlap between the two cases. Assuming that the two ways to trigger are independent, $N_{\text{TIS\&TOS}} = \epsilon_{\text{TIS}}\epsilon_{\text{TOS}}N_{\text{sel}} = N_{\text{TIS}}N_{\text{TOS}}/N_{\text{sel}}$, where, in a given region of phase space, N_{TIS} and N_{TOS} are the number of TIS and TOS events, $N_{\text{TIS\&TOS}}$ is the number of events which are simultaneously both TIS and TOS, and N_{sel} is the number of selected signal events. Hence

$$\epsilon^{\text{trig/sel}}_{\text{data}} = \frac{N_{\text{TIS|TOS}}}{N_{\text{sel}}} = \frac{N_{\text{TIS|TOS}}N_{\text{TIS\&TOS}}}{N_{\text{TIS}}N_{\text{TOS}}}, \tag{9}$$

where $N_{\text{TIS|TOS}}$ is the number of events which are triggered either as TIS or TOS. Due to the limited data statistics, a significant comparison between data and MC can only be done in bands of p_T or y, rather than in 2-dimensional bins. Good agreement is found, as illustrated in Fig. 4 (right), and the observed differences are translated into a global correlated systematic uncertainty of 2%.

The dependence on the modeling of diffractive processes is studied per bin of phase space by changing the fraction of diffractive events in the PYTHIA 6.4 sample by 50% of its value, and by replacing these events with diffractive events generated with PYTHIA 8.1 [15].[1] The evaluation of the MC efficiencies is repeated for different PYTHIA 6.4 parameter values [17], leading to no significant change.

There are two important differences in the analysis of the K^0_S candidates from the long-track selection relative to the downstream-track selection. Firstly, a reconstructed PV is required in the former case, so the systematic uncertainty on the PV reconstruction efficiency needs to be assessed. The simulation is found to be in good agreement with the data, but the analysis is more sensitive to the contribution from diffractive events. Secondly, the background level in the long-track selection is significantly lower than in the downstream-track selection, due to the PV requirement and the precise VELO measurements. Therefore it is possible to remove the minimum p_T requirement on the K^0_S daughters in the long-track selection. This allows the extension of the analysis to two low p_T bins in the range $2.5 < y < 3.0$, which are inaccessible to the downstream-track selection. The dominant systematic error for these two bins is from the large uncertainty on the tracking efficiency for the very low p_T K^0_S daughters.

[1] We consider single- and double-diffractive process types 92–94 in PYTHIA 6.421, which includes only soft diffraction, and 103–105 in PYTHIA 8.130 (soft and hard diffraction).

Table 5
Sources of uncertainty on the K^0_S production cross-sections of Eq. (1), with relative values quoted for the downstream-track selection. A range of values means that the uncertainty was evaluated per bin of (p_T, y) phase space (with extreme values quoted), while a single value indicates a global uncertainty assumed to be bin-independent. The different contributions are classified as uncorrelated or (at least partially) correlated across the different bins.

Source of uncertainty	Uncorrelated	Correlated
Yields N_i^{obs}		
– Data statistics	5–25%	
– Signal extraction	1–5%	
– Beam–gas subtraction		< 1%
Efficiency correction $(\epsilon_i^{\text{trig/sel}}\epsilon_i^{\text{sel}})^{-1}$		
– MC statistics	1–5%	
– Track finding		6–17%
– Selection		4%
– Trigger		2%
– p_T and y shape within bin	0–20%	
– Diffraction modelling		0–1%
– Non-prompt contamination		< 1%
– Material interactions		< 1%
Normalization $(L_{\text{int}})^{-1}$		
– Bunch currents		12%
– Beam widths		5%
– Beam positions		3%
– Beam angles		1%
Sum in quadrature	6–28%	16–23%

The estimates of the total efficiencies $\epsilon_i^{\text{trig/sel}} \times \epsilon_i^{\text{sel}}$ are given in Table 4. The various contributions to the uncertainties have been classified according to their correlations across bins, as shown in Table 5, and added in quadrature.

7. Results and discussion

The cross-sections defined in Eq. (1) are evaluated separately for both the downstream- and long-track selections. In every phase-space bin, the two sets of results are found to be consistent with each other. The relative uncertainties on the measurement for the downstream-track selection are summarized in Table 5. Since the downstream- and long-track results are not statistically independent, and since the downstream-track selection contains already most of the statistical power in bins where a measurement is possible, the measurements are not combined. The final results, listed in Table 6, are taken from the downstream-track selection, except in the two lowest p_T bins for $2.5 < y < 3.0$ where they are taken from the long-track selection.

The corresponding differential cross-sections are shown in Fig. 5 as function of transverse momentum for the three different rapidity bins. They include both non-diffractive and diffractive prompt K^0_S production, and are compared with three different sets of predictions, all obtained with the PYTHIA 6.4 generator [13]. These predictions are represented as histograms in Fig. 5 and correspond to:

Table 6
Prompt K^0_S production cross-section (in μb) measured in bins of transverse momentum p_T and rapidity y, as defined in Eq. (1). The first quoted error is the statistical uncertainty, the second error is the uncorrelated systematic uncertainty, and the third error is the systematic uncertainty correlated across bins.

p_T [GeV/c]	$2.5 < y < 3.0$	$3.0 < y < 3.5$	$3.5 < y < 4.0$
0.0–0.2	$294 \pm 80 \pm 38 \pm 90$	$316 \pm 43 \pm 44 \pm 72$	$196 \pm 39 \pm 39 \pm 38$
0.2–0.4	$649 \pm 133 \pm 136 \pm 183$	$562 \pm 42 \pm 22 \pm 101$	$571 \pm 42 \pm 25 \pm 114$
0.4–0.6	$618 \pm 63 \pm 66 \pm 97$	$534 \pm 30 \pm 12 \pm 86$	$477 \pm 26 \pm 14 \pm 77$
0.6–0.8	$401 \pm 32 \pm 18 \pm 64$	$371 \pm 21 \pm 9 \pm 59$	$323 \pm 20 \pm 9 \pm 51$
0.8–1.0	$232 \pm 20 \pm 4 \pm 37$	$183 \pm 14 \pm 6 \pm 29$	$201 \pm 16 \pm 6 \pm 33$
1.0–1.2	$115 \pm 11 \pm 4 \pm 18$	$136 \pm 11 \pm 3 \pm 22$	$108 \pm 12 \pm 5 \pm 17$
1.2–1.4	$85 \pm 10 \pm 3 \pm 14$	$70 \pm 8 \pm 2 \pm 11$	$35 \pm 9 \pm 3 \pm 6$
1.4–1.6	$46 \pm 7 \pm 2 \pm 7$	$49 \pm 6 \pm 3 \pm 8$	$23 \pm 6 \pm 2 \pm 4$

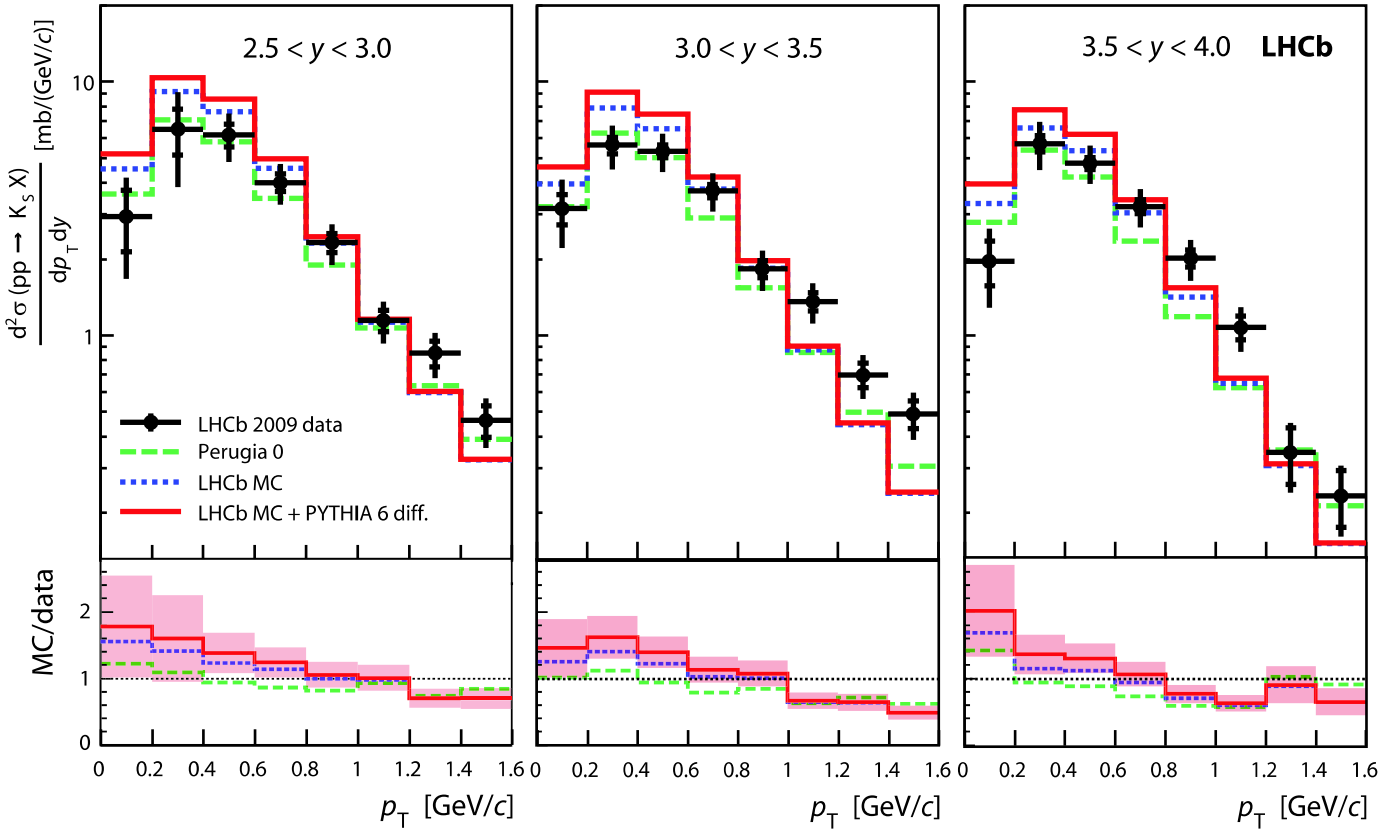

Fig. 5. Double-differential prompt K^0_S production cross-section in pp collisions at $\sqrt{s} = 0.9$ TeV as a function of transverse momentum p_T and rapidity y. The points represent LHCb data, with total uncertainties shown as vertical error bars and statistical uncertainties as tick marks on the bars. The histograms are predictions from different settings of the PYTHIA generator (see text). The lower plots show the MC/data ratios, with the shaded band representing the uncertainty for one of these ratios, dominated by the uncertainty on the measurements (the relative uncertainties for the other ratios are similar).

- the LHCb settings,[2] which include only soft diffraction as described by PYTHIA 6.4 (red solid histogram);
- the LHCb settings where diffractive processes have been switched off (blue dotted histogram);
- the "Perugia 0" settings [17], which exclude diffraction (green dashed histogram).

The predictions agree reasonably well with the data, although they tend to underestimate (overestimate) the measured production in the highest (lowest) p_T bins.

Previous measurements of the prompt K^0_S cross-section in high-energy $p\bar{p}$ collisions, performed by UA5 [2], UA1 [5] and CDF [4] at different centre-of-mass energies and in different rapidity or pseudo-rapidity regions, have been published in the form of invariant differential cross-sections $E\,\mathrm{d}^3\sigma/\mathrm{d}^3p$ as a function of p_T. We convert these into measurements of $\mathrm{d}^2\sigma/(\mathrm{d}p_T\mathrm{d}y)$ by multiplication with $2\pi\,p_T$, and compare them with our results in Fig. 6, lim-

[2] We use PYTHIA 6.421, and include process types 11–13, 28, 53, 68, 91–95, 421–439, 461–479 with non-default parameter values ckin(41) = 3.0, mstp(2) = 2, mstp(33) = 3, mstp(128) = 2, mstp(81) = 21, mstp(82) = 3, mstp(52) = 2, mstp(51) = 10042, parp(67) = 1.0, parp(82) = 4.28, parp(89) = 14000, parp(90) = 0.238, parp(85) = 0.33, parp(86) = 0.66, parp(91) = 1.0, parp(149) = 0.02, parp(150) = 0.085, parj(11) = 0.5, parj(12) = 0.4, parj(13) = 0.79, parj(14) = 0.0, parj(15) = 0.018, parj(16) = 0.054, parj(17) = 0.131, mstj(26) = 0, parj(33) = 0.4. The particle decay probabilities are computed using EvtGen [16].

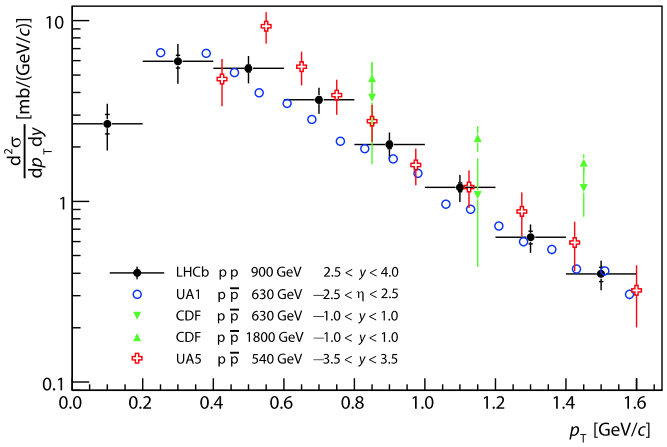

Fig. 6. Absolute measurements of the prompt K^0_S production cross-section as a function of transverse momentum p_T, performed by the UA1 [5], UA5 [2], CDF [4] and LHCb experiments, at different high-energy hadron colliders and in different rapidity (y) or pseudo-rapidity (η) ranges.

iting the p_T range of previous measurements to 1.6 GeV/c. In this figure, LHCb results are shown for the rapidity range $2.5 < y < 4.0$, obtained by averaging the results for the three separate y bins, assuming conservatively that the correlated systematic uncertainties are 100% correlated. In general the agreement is reasonable, given the spread of centre-of-mass energies and the fact that the results are averaged over different ranges in rapidity or pseudo-rapidity. The ability of LHCb to contribute measurements that extend the kinematic range towards high rapidities and very low p_T is apparent.

8. Conclusions

Studies of prompt K^0_S production at $\sqrt{s} = 0.9$ TeV have been presented, made with the LHCb detector using the first pp collisions delivered by the LHC during 2009. The data sample used corresponds to an integrated luminosity of $6.8 \pm 1.0\ \mu b^{-1}$, a value which has been determined using measurements of the beam profiles that exploit the high precision of the VELO. This is the most precise determination of the luminosity for the 2009 LHC pilot run, only limited by the uncertainties on the beam intensity.

The differential cross-section has been measured as a function of p_T and y, over a range extending down to p_T less than 0.2 GeV/c, and in the rapidity interval $2.5 < y < 4.0$, a region that has not been explored in previous experiments at this energy. These results show reasonable consistency with expectations based on the PYTHIA 6.4 generator, and should provide valuable input for the future tuning of Monte Carlo generators.

Acknowledgements

We express our gratitude to our colleagues in the CERN accelerator departments for the excellent performance of the LHC. The valuable contribution of J.-J. Gras (CERN) to the analysis of the LHC beam current measurements is gratefully acknowledged. We thank the technical and administrative staff at CERN and at the LHCb institutes, and acknowledge support from the National Agencies: CAPES, CNPq, FAPERJ and FINEP (Brazil); CERN; NSFC (China); CNRS/IN2P3 (France); BMBF, DFG, HGF and MPG (Germany); SFI (Ireland); INFN (Italy); FOM and NWO (Netherlands); SCSR (Poland); ANCS (Romania); MinES of Russia and Rosatom (Russia); MICINN, XUNGAL and GENCAT (Spain); SNSF and SER (Switzerland); NAS Ukraine (Ukraine); STFC (United Kingdom); NSF (USA). We also acknowledge the support received from the ERC under FP7 and the Région Auvergne.

Open Access

References

[1] D. Drijard, et al., CDHW Collaboration, Z. Phys. C 12 (1982) 217.
[2] G.J. Alner, et al., UA5 Collaboration, Nucl. Phys. B 258 (1985) 505.
[3] R.E. Ansorge, et al., UA5 Collaboration, Z. Phys. C 41 (1988) 179.
[4] F. Abe, et al., CDF Collaboration, Phys. Rev. D 40 (1989) 3791.
[5] G. Bocquet, et al., UA1 Collaboration, Phys. Lett. B 366 (1996) 441.
[6] D. Acosta, et al., CDF Collaboration, Phys. Rev. D 72 (2005) 052001.
[7] B.I. Abelev, et al., STAR Collaboration, Phys. Rev. C 75 (2007) 064901.
[8] A.A. Alves, et al., LHCb Collaboration, JINST 3 (2008) S08005, and references therein.
[9] M. Ferro-Luzzi, Nucl. Instrum. Methods A 553 (2005) 388.
[10] C. Møller, K. Dan. Vidensk. Selsk. Mat. Fys. Medd. 23 (1945) 1.
[11] D. Belohrad, et al., Commissioning and first performance of the LHC beam current measurement systems, MOPE059, Proceedings of the 1st International Particle Accelerator Conference (IPAC 2010), Kyoto, Japan, May 2010.
[12] C. Amsler, et al., Particle Data Group, Phys. Lett. B 667 (2008) 1.
[13] T. Sjöstrand, S. Mrenna, P. Skands, JHEP 0605 (2006) 026.
[14] S. Agostinelli, et al., Nucl. Instrum. Methods A 506 (2003) 250.
[15] S. Navin, Diffraction in PYTHIA, LUTP-09-23, arXiv:1005.3894v1 [hep-ph], May 2010.
[16] D.J. Lange, Nucl. Instrum. Methods A 462 (2001) 152.
[17] P.Z. Skands, The Perugia tunes, CERN-PH-TH-2010-113, arXiv:1005.3457v1 [hep-ph], May 2010.

LHCb Collaboration

R. Aaij [23], C. Abellan Beteta [35,m], B. Adeva [36], M. Adinolfi [42], C. Adrover [6], A. Affolder [48], M. Agari [10], Z. Ajaltouni [5], J. Albrecht [37], F. Alessio [6,37], M. Alexander [47], M. Alfonsi [18], P. Alvarez Cartelle [36], A.A. Alves Jr. [22], S. Amato [2], Y. Amhis [38], J. Amoraal [23], J. Anderson [39], R. Antunes Nobrega [22,k], R. Appleby [50], O. Aquines Gutierrez [10], A. Arefyev [30], L. Arrabito [53], M. Artuso [52], E. Aslanides [6], G. Auriemma [22,l], S. Bachmann [11], Y. Bagaturia [11], D.S. Bailey [50], V. Balagura [30,37], W. Baldini [16], G. Barber [49], C. Barham [43], R.J. Barlow [50], S. Barsuk [7], S. Basiladze [31], A. Bates [47], C. Bauer [10], Th. Bauer [23], A. Bay [38], I. Bediaga [1], T. Bellunato [20,i], K. Belous [34], I. Belyaev [23,30], M. Benayoun [8], G. Bencivenni [18], R. Bernet [39], R.P. Bernhard [39], M.-O. Bettler [17], M. van Beuzekom [23], J.H. Bibby [51], S. Bifani [12], A. Bizzeti [17,g], P.M. Bjørnstad [50], T. Blake [49], F. Blanc [38], C. Blanks [49], J. Blouw [11], S. Blusk [52], A. Bobrov [33], V. Bocci [22], B. Bochin [29], E. Bonaccorsi [37], A. Bondar [33], N. Bondar [29,37], W. Bonivento [15], S. Borghi [47], A. Borgia [52], E. Bos [23], T.J.V. Bowcock [48], C. Bozzi [16], T. Brambach [9], J. van den Brand [24], L. Brarda [37], J. Bressieux [38], S. Brisbane [51], M. Britsch [10], N.H. Brook [42], H. Brown [48], S. Brusa [16], A. Büchler-Germann [39], A. Bursche [39], J. Buytaert [37], S. Cadeddu [15], J.M. Caicedo Carvajal [37], O. Callot [7], M. Calvi [20,i], M. Calvo Gomez [35,m], A. Camboni [35], W. Cameron [49], L. Camilleri [37], P. Campana [18], A. Carbone [14], G. Carboni [21,j], R. Cardinale [19,h], A. Cardini [15], J. Carroll [48], L. Carson [36], K. Carvalho Akiba [23], G. Casse [48], M. Cattaneo [37], B. Chadaj [37], M. Charles [51], Ph. Charpentier [37], J. Cheng [3], N. Chiapolini [39], A. Chlopik [27], J. Christiansen [37], P. Ciambrone [18], X. Cid Vidal [36], P.J. Clark [46], P.E.L. Clarke [46], M. Clemencic [37], H.V. Cliff [43], J. Closier [37], C. Coca [28], V. Coco [52], J. Cogan [6], P. Collins [37], A. Comerma-Montells [35], F. Constantin [28], G. Conti [38], A. Contu [51], P. Cooke [48], M. Coombes [42], B. Corajod [37], G. Corti [37], G.A. Cowan [46], R. Currie [46], B. D'Almagne [7], C. D'Ambrosio [37], I. D'Antone [14], W. Da Silva [8], E. Dane' [18], P. David [8], I. De Bonis [4], S. De Capua [21,j], M. De Cian [39], F. De Lorenzi [12], J.M. De Miranda [1], L. De Paula [2], P. De Simone [18], D. Decamp [4], G. Decreuse [37], H. Degaudenzi [38,37], M. Deissenroth [11], L. Del Buono [8], C.J. Densham [45], C. Deplano [15], O. Deschamps [5], F. Dettori [15,c], J. Dickens [43], H. Dijkstra [37], M. Dima [28], S. Donleavy [48], P. Dornan [49], D. Dossett [44], A. Dovbnya [40], R. Dumps [37], F. Dupertuis [38], L. Dwyer [48], R. Dzhelyadin [34], C. Eames [49], S. Easo [45], U. Egede [49], V. Egorychev [30], S. Eidelman [33], D. van Eijk [23], F. Eisele [11], S. Eisenhardt [46], L. Eklund [47], D.G. d'Enterria [35,n], D. Esperante Pereira [36], L. Estève [43], E. Fanchini [20,i], C. Färber [11], G. Fardell [46], C. Farinelli [23], S. Farry [12], V. Fave [38], G. Felici [18], V. Fernandez Albor [36], M. Ferro-Luzzi [37], S. Filippov [32], C. Fitzpatrick [46], W. Flegel [37], F. Fontanelli [19,h], C. Forti [18], R. Forty [37], C. Fournier [37], B. Franek [45], M. Frank [37], C. Frei [37], M. Frosini [17,e], J.L. Fungueirino Pazos [36], S. Furcas [20], A. Gallas Torreira [36], D. Galli [14,b], M. Gandelman [2], P. Gandini [51], Y. Gao [3], J.-C. Garnier [37], L. Garrido [35], D. Gascon [35], C. Gaspar [37], A. Gaspar De Valenzuela Cue [35,m], J. Gassner [39], N. Gauvin [38], P. Gavillet [37], M. Gersabeck [37], T. Gershon [44], Ph. Ghez [4], V. Gibson [43], Yu. Gilitsky [34,†], V.V. Gligorov [37], C. Göbel [54], D. Golubkov [30], A. Golutvin [49,30,37], A. Gomes [1], G. Gong [3], H. Gong [3], H. Gordon [51], M. Grabalosa Gándara [35], V. Gracco [19,h], R. Graciani Diaz [35], L.A. Granado Cardoso [37], E. Graugés [35], G. Graziani [17], A. Grecu [28], S. Gregson [43], G. Guerrer [1], B. Gui [52], E. Gushchin [32], Yu. Guz [34,37], Z. Guzik [27], T. Gys [37], G. Haefeli [38], S.C. Haines [43], T. Hampson [42], S. Hansmann-Menzemer [11], R. Harji [49], N. Harnew [51], P.F. Harrison [44], J. He [7], K. Hennessy [48], P. Henrard [5], J.A. Hernando Morata [36], E. van Herwijnen [37], A. Hicheur [38], E. Hicks [48], H.J. Hilke [37], W. Hofmann [10], K. Holubyev [11], P. Hopchev [4], W. Hulsbergen [23], P. Hunt [51], T. Huse [48], R.S. Huston [12], D. Hutchcroft [48], F. Iacoangeli [22], V. Iakovenko [7,41], C. Iglesias Escudero [36], C. Ilgner [9], J. Imong [42], R. Jacobsson [37], M. Jahjah Hussein [5], O. Jamet [37], E. Jans [23], F. Jansen [23], P. Jaton [38], B. Jean-Marie [7], M. John [51], D. Johnson [51], C.R. Jones [43], B. Jost [37], F. Kapusta [8], T.M. Karbach [9], A. Kashchuk [29], S. Katvars [43], J. Keaveney [12], U. Kerzel [43], T. Ketel [24], A. Keune [38], S. Khalil [52], B. Khanji [6], Y.M. Kim [46], M. Knecht [38], S. Koblitz [37], A. Konoplyannikov [30], P. Koppenburg [23], M. Korolev [31], A. Kozlinskiy [23], L. Kravchuk [32], R. Kristic [37], G. Krocker [11], P. Krokovny [11], F. Kruse [9], K. Kruzelecki [37], M. Kucharczyk [25], I. Kudryashov [31], S. Kukulak [25], R. Kumar [14], T. Kvaratskheliya [30], V.N. La Thi [38], D. Lacarrere [37], A. Lai [15], R.W. Lambert [37], G. Lanfranchi [18], C. Langenbruch [11], T. Latham [44], R. Le Gac [6], J.-P. Lees [4], R. Lefèvre [5], A. Leflat [31,37], J. Lefrançois [7], F. Lehner [39], M. Lenzi [17], O. Leroy [6], T. Lesiak [25], L. Li [3], Y.Y. Li [43], L.Li Gioi [5], J. Libby [51], M. Lieng [9], R. Lindner [37], S. Lindsey [48], C. Linn [11], B. Liu [3], G. Liu [37], S. Löchner [10], J.H. Lopes [2], E. Lopez Asamar [35], N. Lopez-March [38], P. Loveridge [45], J. Luisier [38], B. M'charek [24], F. Machefert [7], I.V. Machikhiliyan [4,30], F. Maciuc [10], O. Maev [29], J. Magnin [1], A. Maier [37],

S. Malde [51], R.M.D. Mamunur [37], G. Manca [15,c], G. Mancinelli [6], N. Mangiafave [43], U. Marconi [14], R. Märki [38], J. Marks [11], G. Martellotti [22], A. Martens [7], L. Martin [51], D. Martinez Santos [36], A. Massaferri [1], Z. Mathe [12], C. Matteuzzi [20], V. Matveev [34], E. Maurice [6], B. Maynard [52], A. Mazurov [32], G. McGregor [50], R. McNulty [12], C. Mclean [14], M. Merk [23], J. Merkel [9], M. Merkin [31], R. Messi [21,j], F.C.D. Metlica [42], S. Miglioranzi [37], M.-N. Minard [4], G. Moine [37], S. Monteil [5], D. Moran [12], J. Morant [37], J.V. Morris [45], J. Moscicki [37], R. Mountain [52], I. Mous [23], F. Muheim [46], R. Muresan [38], F. Murtas [18], B. Muryn [26], M. Musy [35], J. Mylroie-Smith [48], P. Naik [42], T. Nakada [38], R. Nandakumar [45], J. Nardulli [45], A. Nawrot [27], M. Nedos [9], M. Needham [38], N. Neufeld [37], P. Neustroev [29], M. Nicol [7], L. Nicolas [38], S. Nies [9], V. Niess [5], N. Nikitin [31], A. Noor [48], A. Oblakowska-Mucha [26], V. Obraztsov [34], S. Oggero [23], O. Okhrimenko [41], R. Oldeman [15,c], M. Orlandea [28], A. Ostankov [34], J. Palacios [23], M. Palutan [18], J. Panman [37], A. Papadelis [23], A. Papanestis [45], M. Pappagallo [13,a], C. Parkes [47], C.J. Parkinson [49], G. Passaleva [17], G.D. Patel [48], M. Patel [49], S.K. Paterson [49,37], G.N. Patrick [45], C. Patrignani [19,h], E. Pauna [28], C. Pauna (Chiojdeanu) [28], C. Pavel (Nicorescu) [28], A. Pazos Alvarez [36], A. Pellegrino [23], G. Penso [22,k], M. Pepe Altarelli [37], S. Perazzini [14,b], D.L. Perego [20,i], E. Perez Trigo [36], A. Pérez-Calero Yzquierdo [35], P. Perret [5], G. Pessina [20], A. Petrella [16,d], A. Petrolini [19,h], E. Picatoste Olloqui [35], B. Pie Valls [35], D. Piedigrossi [37], B. Pietrzyk [4], D. Pinci [22], S. Playfer [46], M. Plo Casasus [36], M. Poli-Lener [18], G. Polok [25], A. Poluektov [44,33], E. Polycarpo [2], D. Popov [10], B. Popovici [28], S. Poss [6], C. Potterat [38], A. Powell [51], S. Pozzi [16,d], T. du Pree [23], V. Pugatch [41], A. Puig Navarro [35], W. Qian [3,7], J.H. Rademacker [42], B. Rakotomiaramanana [38], I. Raniuk [40], G. Raven [24], S. Redford [51], W. Reece [49], A.C. dos Reis [1], S. Ricciardi [45], J. Riera [35,m], K. Rinnert [48], D.A. Roa Romero [5], P. Robbe [7,37], E. Rodrigues [47], F. Rodrigues [2], C. Rodriguez Cobo [36], P. Rodriguez Perez [36], G.J. Rogers [43], V. Romanovsky [34], E. Rondan Sanabria [1], M. Rosello [35,m], G. Rospabe [4], J. Rouvinet [38], L. Roy [37], T. Ruf [37], H. Ruiz [35], C. Rummel [11], V. Rusinov [30], G. Sabatino [21,j], J.J. Saborido Silva [36], N. Sagidova [29], P. Sail [47], B. Saitta [15,c], T. Sakhelashvili [39], C. Salzmann [39], A. Sambade Varela [37], M. Sannino [19,h], R. Santacesaria [22], R. Santinelli [37], E. Santovetti [21,j], M. Sapunov [6], A. Sarti [18], C. Satriano [22,l], A. Satta [21], T. Savidge [49], M. Savrie [16,d], D. Savrina [30], P. Schaack [49], M. Schiller [11], S. Schleich [9], M. Schmelling [10], B. Schmidt [37], O. Schneider [38,*], T. Schneider [37], A. Schopper [37], M.-H. Schune [7], R. Schwemmer [37], A. Sciubba [18,k], M. Seco [36], A. Semennikov [30], K. Senderowska [26], N. Serra [23], J. Serrano [6], B. Shao [3], M. Shapkin [34], I. Shapoval [40,37], P. Shatalov [30], Y. Shcheglov [29], T. Shears [48], L. Shekhtman [33], V. Shevchenko [30], A. Shires [49], S. Sigurdsson [43], E. Simioni [24], H.P. Skottowe [43], T. Skwarnicki [52], N. Smale [10,51], A. Smith [37], A.C. Smith [37], N.A. Smith [48], K. Sobczak [5], F.J.P. Soler [47], A. Solomin [42], P. Somogy [37], F. Soomro [49], B. Souza De Paula [2], B. Spaan [9], A. Sparkes [46], E. Spiridenkov [29], P. Spradlin [51], A. Srednicki [27], F. Stagni [37], S. Stahl [11], S. Steiner [39], O. Steinkamp [39], O. Stenyakin [34], S. Stoica [28], S. Stone [52], B. Storaci [23], U. Straumann [39], N. Styles [46], M. Szczekowski [27], P. Szczypka [38], T. Szumlak [47,26], S. T'Jampens [4], E. Tarkovskiy [30], E. Teodorescu [28], H. Terrier [23], F. Teubert [37], C. Thomas [51,45], E. Thomas [37], J. van Tilburg [39], V. Tisserand [4], M. Tobin [39], S. Topp-Joergensen [51], M.T. Tran [38], S. Traynor [12], U. Trunk [10], A. Tsaregorodtsev [6], N. Tuning [23], A. Ukleja [27], O. Ullaland [37], U. Uwer [11], V. Vagnoni [14], G. Valenti [14], A. Van Lysebetten [23], R. Vazquez Gomez [35], P. Vazquez Regueiro [36], S. Vecchi [16], J.J. Velthuis [42], M. Veltri [17,f], K. Vervink [37], B. Viaud [7], I. Videau [7], D. Vieira [2], X. Vilasis-Cardona [35,m], J. Visniakov [36], A. Vollhardt [39], D. Volyanskyy [39], D. Voong [42], A. Vorobyev [29], An. Vorobyev [29], H. Voss [10], K. Wacker [9], S. Wandernoth [11], J. Wang [52], D.R. Ward [43], A.D. Webber [50], D. Websdale [49], M. Whitehead [44], D. Wiedner [11], L. Wiggers [23], G. Wilkinson [51], M.P. Williams [44], M. Williams [49], F.F. Wilson [45], J. Wishahi [9], M. Witek [25], W. Witzeling [37], M.L. Woodward [45], S.A. Wotton [43], K. Wyllie [37], Y. Xie [46], F. Xing [51], Z. Yang [3], G. Ybeles Smit [23], R. Young [46], O. Yushchenko [34], M. Zeng [3], L. Zhang [52], Y. Zhang [3], A. Zhelezov [11], E. Zverev [31]

[1] *Centro Brasileiro de Pesquisas Físicas (CBPF), Rio de Janeiro, Brazil*
[2] *Universidade Federal do Rio de Janeiro (UFRJ), Rio de Janeiro, Brazil*
[3] *Center for High Energy Physics, Tsinghua University, Beijing, China*
[4] *LAPP, Université de Savoie, CNRS/IN2P3, Annecy-Le-Vieux, France*
[5] *Clermont Université, Université Blaise Pascal, CNRS/IN2P3, LPC, Clermont-Ferrand, France*
[6] *CPPM, Aix-Marseille Université, CNRS/IN2P3, Marseille, France*
[7] *LAL, Université Paris-Sud, CNRS/IN2P3, Orsay, France*
[8] *LPNHE, Université Pierre et Marie Curie, Université Paris Diderot, CNRS/IN2P3, Paris, France*
[9] *Fakultät Physik, Technische Universität Dortmund, Dortmund, Germany*
[10] *Max-Planck-Institut für Kernphysik (MPIK), Heidelberg, Germany*
[11] *Physikalisches Institut, Ruprecht-Karls-Universität Heidelberg, Heidelberg, Germany*
[12] *School of Physics, University College Dublin, Dublin, Ireland*

[13] *Sezione INFN di Bari, Bari, Italy*
[14] *Sezione INFN di Bologna, Bologna, Italy*
[15] *Sezione INFN di Cagliari, Cagliari, Italy*
[16] *Sezione INFN di Ferrara, Ferrara, Italy*
[17] *Sezione INFN di Firenze, Firenze, Italy*
[18] *Laboratori Nazionali dell'INFN di Frascati, Frascati, Italy*
[19] *Sezione INFN di Genova, Genova, Italy*
[20] *Sezione INFN di Milano Bicocca, Milano, Italy*
[21] *Sezione INFN di Roma Tor Vergata, Roma, Italy*
[22] *Sezione INFN di Roma Sapienza, Roma, Italy*
[23] *Nikhef National Institute for Subatomic Physics, Amsterdam, Netherlands*
[24] *Nikhef National Institute for Subatomic Physics and Vrije Universiteit, Amsterdam, Netherlands*
[25] *Henryk Niewodniczanski Institute of Nuclear Physics, Polish Academy of Sciences, Cracow, Poland*
[26] *Faculty of Physics & Applied Computer Science, Cracow, Poland*
[27] *Soltan Institute for Nuclear Studies, Warsaw, Poland*
[28] *Horia Hulubei National Institute of Physics and Nuclear Engineering, Bucharest–Magurele, Romania*
[29] *Petersburg Nuclear Physics Institute (PNPI), Gatchina, Russia*
[30] *Institute of Theoretical and Experimental Physics (ITEP), Moscow, Russia*
[31] *Institute of Nuclear Physics, Moscow State University (SINP MSU), Moscow, Russia*
[32] *Institute for Nuclear Research of the Russian Academy of Sciences (INR RAN), Moscow, Russia*
[33] *Budker Institute of Nuclear Physics (BINP), Novosibirsk, Russia*
[34] *Institute for High Energy Physics (IHEP), Protvino, Russia*
[35] *Universitat de Barcelona, Barcelona, Spain*
[36] *Universidad de Santiago de Compostela, Santiago de Compostela, Spain*
[37] *European Organization for Nuclear Research (CERN), Geneva, Switzerland*
[38] *Ecole Polytechnique Fédérale de Lausanne (EPFL), Lausanne, Switzerland*
[39] *Physik Institut, Universität Zürich, Zürich, Switzerland*
[40] *NSC Kharkiv Institute of Physics and Technology (NSC KIPT), Kharkiv, Ukraine*
[41] *Institute for Nuclear Research of the National Academy of Sciences (KINR), Kyiv, Ukraine*
[42] *H.H. Wills Physics Laboratory, University of Bristol, Bristol, United Kingdom*
[43] *Cavendish Laboratory, University of Cambridge, Cambridge, United Kingdom*
[44] *Department of Physics, University of Warwick, Coventry, United Kingdom*
[45] *STFC Rutherford Appleton Laboratory, Didcot, United Kingdom*
[46] *School of Physics and Astronomy, University of Edinburgh, Edinburgh, United Kingdom*
[47] *School of Physics and Astronomy, University of Glasgow, Glasgow, United Kingdom*
[48] *Oliver Lodge Laboratory, University of Liverpool, Liverpool, United Kingdom*
[49] *Imperial College London, London, United Kingdom*
[50] *School of Physics and Astronomy, University of Manchester, Manchester, United Kingdom*
[51] *Department of Physics, University of Oxford, Oxford, United Kingdom*
[52] *Syracuse University, Syracuse, NY, United States*
[53] *CC-IN2P3, CNRS/IN2P3, Lyon-Villeurbanne, France* [o]
[54] *Pontifícia Universidade Católica do Rio de Janeiro (PUC-Rio), Rio de Janeiro, Brazil* [p]

* Corresponding author.
E-mail address: Olivier.Schneider@epfl.ch (O. Schneider).
[†] Deceased.
[a] Università di Bari, Bari, Italy.
[b] Università di Bologna, Bologna, Italy.
[c] Università di Cagliari, Cagliari, Italy.
[d] Università di Ferrara, Ferrara, Italy.
[e] Università di Firenze, Firenze, Italy.
[f] Università di Urbino, Urbino, Italy.
[g] Università di Modena e Reggio Emilia, Modena, Italy.
[h] Università di Genova, Genova, Italy.
[i] Università di Milano Bicocca, Milano, Italy.
[j] Università di Roma Tor Vergata, Roma, Italy.
[k] Università di Roma La Sapienza, Roma, Italy.
[l] Università della Basilicata, Potenza, Italy.
[m] LIFAELS, La Salle, Universitat Ramon Llull, Barcelona, Spain.
[n] Institució Catalana de Recerca i Estudis Avançats (ICREA), Barcelona, Spain.
[o] Associated member.
[p] Associated to Universidade Federal do Rio de Janeiro (UFRJ), Rio de Janeiro, Brazil.